Contribution from the Department of Physical Chemistry, University of Nijmegen, Toernooiveld, 6525 ED Nijmegen, The Netherlands, and the Departments of Chemistry, University of Massachusetts, Amherst, Massachusetts 01003, and Brookhaven National Laboratory, Upton, New York 11973

Structure Determinations of the Low-Temperature Phases of the Copper Pyridine *N*-Oxide Complexes $Cu(C_5H_5NO)_6X_2$ by Neutron Diffraction and EPR: Influence of Solvent and Anion on the Nature of the Cooperative Jahn–Teller Coupling

C. P. KEIJZERS,[1a] R. K. McMULLAN,[1b] J. S. WOOD,*[1c] G. VAN KALKEREN,[1a] R. SRINIVASAN,[1d] and E. DE BOER[1a]

Received January 12, 1982

The hexakis(pyridine *N*-oxide)copper fluoborate and perchlorate complexes have been examined by single-crystal neutron diffraction, electron paramagnetic resonance, and magnetic susceptibility measurements, in order to elucidate the nature of the cooperative Jahn–Teller effect (CJTE) exhibited by these salts and its dependence on the nature of the anion and the solvent used for crystal growing. Neutron diffraction studies between 298 and 20 K on crystals of the fluoborate salt and of the perchlorate salt grown from acetonitrile solution confirm the loss of the high-temperature $\bar{3}$ symmetry of the crystals and the formation of three domains associated with static Jahn–Teller-distorted structures at temperatures of ca. 60 K, as was earlier indicated by EPR results. However, although single-crystal susceptibility measurements of the ClO_4^- salt grown from dimethylformamide solution indicate a phase change associated with a Jahn–Teller transition, the diffraction studies show that the $\bar{3}$ symmetry is retained to 20 K. At 20 K, this salt is rhombohedral, space group $R\bar{3}$, with lattice dimensions $a = 12.260$ (1) Å, $c = 18.798$ (2) Å, and three molecules per hexagonal unit cell. The structure has been refined with use of 1938 neutron reflection intensities ($(\sin\theta)/\lambda \leq 0.79$ Å^{-1}) recorded at 20 K, the final $R(F^2)$ and $R_w(F^2)$ values being 0.041 and 0.047, respectively. The analysis indicates that DMF molecules are incorporated statistically into the complex, to the extent of approximately 1 molecule to 40 pyridine *N*-oxide molecules. The DMF molecules occupy tetragonal distortion sites about the copper, with Cu–O distances of 2.67 Å, and the presence of these tetragonally distorted complexes in samples grown from DMF solution explains the appearance of the static sites in the earlier reported room-temperature EPR spectra of doped crystals containing $Cu(C_5H_5NO)_6^{2+}$. The main structure is interpreted in terms of a statistically averaged static Jahn–Teller distortion for the $Cu(C_5H_5NO)_6^{2+}$ ion, and analysis of the atomic thermal parameters gives a Jahn–Teller radius of 0.34 Å. Single crystals and powders of mixed salts with varying ClO_4^-/BF_4^- ratios and heavily doped single crystals of the isostructural zinc complexes have been examined by EPR techniques to assess the relative stabilities of the low-temperature ferrodistortive and antiferrodistortive forms characteristic respectively of the BF_4^- and ClO_4^- salts. The measurements on the mixed salts reveal the presence of both forms and suggest that the latter is the energetically more favorable one, while the single-crystal EPR measurements on 10% $^{63}Cu/Zn(C_5H_5NO)_6^{2+}$ salts indicate the presence of copper pairs and also confirm that the antiferrodistortive phase is the more stable one: the spectra for the fluoborate complex show lines attributable to antiferrodistortive pairs, in addition to spectra arising from ferrodistortively coupled pairs, while crystals of the perchlorate complex, grown from either acetonitrile or DMF, show almost exclusively the former pair lines. The influence of the solvated species in modifying the normal ferrodistortive and antiferrodistortive behavior is discussed, and structural models for the low-temperature phases incorporating these species are proposed.

Introduction

Together with the hexanitro complexes of copper(II) $M_2M'Cu(NO_2)_6$,[2] the hexakis(pyridine *N*-oxide) salts $Cu(C_5H_5NO)_6X_2$ provide one of the more interesting series of discrete six-coordinate copper complexes exhibiting both static-cooperative and dynamic Jahn–Teller effects. While crystals of the high-temperature phases of these salts do not possess as high a symmetry as those of the nitro complexes, being rhombohedral rather than cubic, they do have the advantage of being isostructural with those of the analogous zinc complex, so that EPR studies of the doped systems are possible. Previous papers have described the room-temperature crystal structures of the $Cu(C_5H_5NO)_6X_2$ salts,[3-5] variable-temperature EPR measurements on both the pure and zinc-doped complexes,[3,6-9] and magnetic susceptibility[3,7] and magnetic specific heat measurements.[10] These latter results have been interpreted in terms of $S = {}^1/_2$, planar and linear chain Heisenberg antiferromagnetism for the fluoborate and perchlorate salts, respectively. Two low-temperature structural models have been postulated,[8,9] which account for these results and for the powder and single-crystal EPR measurements made below the Jahn–Teller transition temperature. These models are derived from the room-temperature structure of $\bar{3}$ symmetry and incorporate two different cooperative orderings induced by Jahn–Teller distortions. They are illustrated in Figure 1. With the assumption of magnetic exchange between neighboring ions, they lead to very different crystal **g** tensors. In the first (the ferrodistortive) model, the distorted complexes have their tetragonal axes parallel, and thus the crystal and molecular tensors are equivalent, while for the second (the antiferrodistortive) model, the tetragonal axes of nearest-neighbor complexes are mutually orthogonal, and the so-called "reversed" **g**-tensor behavior ($g_\perp > g_\parallel$) is expected. As a result, the crystal and molecular tensors are no longer equivalent.[11] We have found that all crystals of the fluoborate complex conform to the former type of behavior, while only crystals of the perchlorate complex grown from ethanol or acetonitrile conform to the latter type, three nonequivalent antiferrodistortive domains, related by the crystal trigonal axis, being produced below the Jahn–Teller transition temperature. Those ClO_4 crystals grown from DMF solution exhibit entirely

(1) (a) University of Nijmegen. (b) Brookhaven National Laboratory. (c) University of Massachusetts. (d) On leave from the Department of Physics, Indian Institute of Science, Bangalore 560012, India, to the University of Nijmegen, 1980–1981.
(2) For a review of the work on these compounds and for a summary of the terminology associated with the Jahn–Teller effect and used here, see: Reinen, D.; Friebel, C. *Struct. Bonding (Berlin)* **1979**, *37*, 1 and references cited therein.
(3) Taylor, D. *Aust. J. Chem.* **1978**, *31*, 713.
(4) O'Connor, C. J.; Sinn, E.; Carlin, R. L. *Inorg. Chem.* **1977**, *16*, 3314.
(5) Day, R. O.; Wood, J. S. *Cryst. Struct. Commun.* **1981**, *10*, 255.
(6) de Boer, E.; Keijzers, C. P.; Wood, J. S. *Chem. Phys. Lett.* **1977**, *53*, 489.
(7) Wood, J. S.; de Boer, E.; Keijzers, C. P. *Inorg. Chem.* **1979**, *18*, 904.
(8) Reinen, D.; Krause, S. *Solid State Commun.* **1979**, *29*, 691.
(9) Wood, J. S.; Keijzers, C. P.; de Boer, E.; Buttafava, A. *Inorg. Chem.* **1980**, *19*, 2213.
(10) Algra, H. A.; de Jongh, L. J.; Carlin, R. L. *Physica B + C (Amsterdam)* **1978**, *93B+C*, 24.
(11) In the case of the $Cu(C_5H_5NO)_6^{2+}$ complexes, the crystal and molecular **g** tensors are slightly rhombic rather than axial, since the low-temperature structures derived from $R\bar{3}$ will have only triclinic symmetry and the complexes $\bar{1}$ symmetry.

0020-1669/82/1321-4275$01.25/0

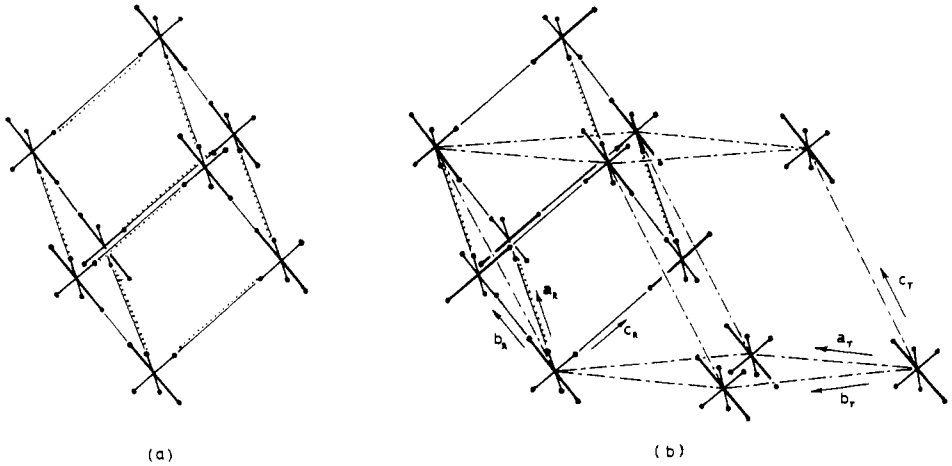

Figure 1. Rhombohedral unit cell of $Cu(C_5H_5NO)_6X_2$ complexes showing the proposed low-temperature structures for (a) the fluoborate complex (ferrodistortive) and (b) the perchlorate complex (antiferrodistortive). In (b) the pseudo-body-centered triclinic unit cell of two molecules is indicated by broken lines. The dotted lines denote the directions of principal antiferromagnetic exchange between neighboring complexes.

different EPR behavior, showing no clear evidence of the dynamic to static Jahn–Teller transition which is manifested in all the other crystals by a change from one isotropic to three anisotropic signals. At all temperatures from 295 to 4 K, the spectrum consists solely of one exchange-narrowed line based on an axial **g** tensor with $g_\perp > g_\parallel$. Assuming that a dynamic–static Jahn–Teller transition had indeed occurred for this phase, we proposed in our previous paper[9] an alternative antiferrodistortive coupling model in the trigonal space group $P3_1$, which accounted for this behavior and which was also consistent with the observed linear-chain magnetism.[4] Since it seemed clear from our EPR measurements on the zinc-doped systems[6,7] that in crystals grown from DMF a certain amount of solvation takes place, to give respectively small amounts of $Cu(C_5H_5NO)_5(DMF)^{2+}$ and $Cu(C_5H_5NO)_4(DMF)_2^{2+}$, we presumed that solvation was occurring for the pure salts. However, since mass spectroscopic measurements suggested that only a very small number (ca. 1 in 10^3) of complexes were solvated, our proposed model for the second antiferrodistortive phase did not include any of these molecules.

In order to shed more light on the nature of the low-temperature structure of the DMF-grown crystals and to confirm the formation of the low-temperature three-domain structures for the crystals grown from other solvents, proposed on the basis of EPR measurements,[8,9] we have now undertaken neutron diffraction measurements between 20 and 295 K on samples of both fluoborate and perchlorate salts and have completed an analysis of the 20 K structure of the crystals of the perchlorate salt grown from DMF solution. In addition, we have carried out further EPR measurements in order to assess the relative stabilities of the ferro- and antiferrodistortive phases and in an attempt to resolve the dichotomy described above and some discrepancies noted earlier[8,9] regarding the transition temperatures of the various salts. These measurements have been made on single-crystal and powder samples of mixed-salt complexes containing varying ratios of fluoborate and perchlorate anions and on doped single crystals of the zinc complexes of both salts containing a high proportion of ^{63}Cu. The latter measurements were made in order to study the spectra arising from isolated pairs of coupled complexes.

Experimental Section

(a) Sample Preparation. All complexes were prepared according to literature methods.[12] Single crystals of the pure copper and ^{63}Cu-doped zinc salts were grown from different solvents as previously described.[9] Complexes with varying ClO_4^-/BF_4^- ratios were recrystallized from salt mixtures of appropriate composition or, in the case of the 1/1 mixture, were crystallized directly from equimolar amounts of the hydrated copper salts.

(b) Neutron Diffraction Studies. The diffraction data were measured on the automated four-circle diffractometers at the Brookhaven High Flux Beam Reactor. Monochromated neutron beams were obtained by (002) reflection from a beryllium crystal for study of the ClO_4^- salts, and by (220) reflection from a germanium crystal for study of the BF_4^- salt. The respective wavelengths of 1.0442 (2) and 1.1621 (2) Å were calibrated against a standard KBr crystal (a_0 = 6.6000 (13) Å at 298 K). The sample crystals were attached to aluminum pins with rubber cement and sealed inside helium-filled aluminum containers. These were cooled inside a closed-cycle helium refrigerator (Air Products and Chemicals, Inc., DISPLEX Model CS-202), which was mounted within the diffractometer χ circle. Crystal temperatures were measured by means of a Pt resistor that had been calibrated against the magnetic phase transition of an FeF_2 crystal.[13] The cooling rates were ~1°/min above 98 K and ~$^1/_2$°/min below to the minimum of 20 K. Lattice changes on cooling were monitored for three complexes representative of the three types of low-temperature EPR behavior described in the Introduction. Evidence for changes from the rhombohedral lattice was sought by recording individual reflection profiles by the ω-scan technique. In order to detect abrupt changes in the unit-cell dimensions during the transitions, we recorded reflection intensities at 20 K for lattice points that violated the extinction condition $-h + k + l = 3n$ for the equivalent triply primitive hexagonal cell.

(i) Ferrodistortive $Cu(C_5H_5NO)_6(BF_4)_2$ Crystals from DMF. The rhombohedral reflections, 382, 04$\bar{3}$, 120, and 100, all showed marked profile broadening between 50 and 55 K, with the two higher angle reflections becoming resolved into three distinct peaks. Cooling to 20 K produced no further pronounced changes in the reflection profiles. The original profile shapes and intensities were reproduced with minor changes when the crystal was warmed to 80 K and thus showed the phase transition to be reversible. The scan profiles, illustrated in Figure 2A for reflection 382 above and below the transition temperature, are similar to those of reflection 04$\bar{3}$, given previously[9] for this salt. Intensity measurements at 20 K made on randomly sampled lattice points showed no violation of the condition $-h + k + l = 3n$ and thus indicated that the phase transition caused no major change in the unit-cell dimensions.

(ii) Antiferrodistortive $Cu(C_5H_5NO)_6(ClO_4)_2$ Crystals from Acetonitrile. The profiles of reflections 530, 6$\bar{5}$1, 40$\bar{3}$, and 210, monitored in this lattice during cooling, showed broadening similar to that described above, but none of these profiles were resolved into three distinct peaks. Those of reflection 530 are reproduced in Figure 2B. The transition was found to be complete at ~60 K and, as for the BF_4^- complex, to be reversible. Since, according to the EPR results, there are in this structure two molecules per unit cell, an attempt was made to detect the additional reflections arising from the triclinic cell, depicted in Figure 1b. The cell is related to the rhombohedral cell

(12) Reedijk, J. *Recl. Trav. Chim. Pays-Bas* **1969**, *88*, 499.

(13) Hutchings, M. T.; Schulhof, M. P.; Guggenheim, H. J. *Phys. Rev. B: Solid State* **1972**, *5*, 150.

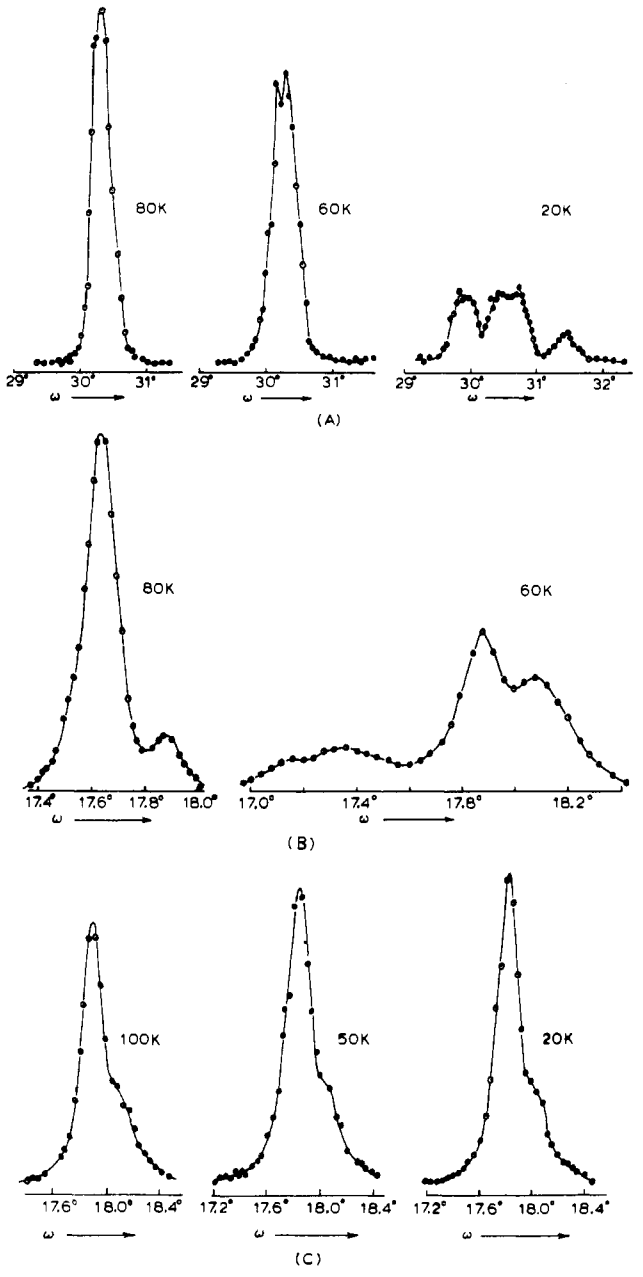

Figure 2. ω scans of neutron reflections from $Cu(C_5H_5NO)_6X_2$ complexes and their temperature dependence: (A) $X = BF_4^-$, 382 reflection, $(\sin\theta)/\lambda = 0.4352$ Å^{-1}; (B) $X = ClO_4^-$, crystal from acetonitrile, 530 reflection, $(\sin\theta)/\lambda = 0.2928$ Å^{-1}; (C) $X = ClO_4^-$, crystal from DMF, 350 reflection, $(\sin\theta)/\lambda = 0.2928$ Å^{-1}. The shoulders observed at high angle in scans B and C are attributed to the beryllium monochromator, rather than to the samples.

as follows: $\vec{a}_T = \vec{a}_R - \vec{c}_R$, $\vec{b}_T = \vec{b}_R - \vec{c}_R$, and $\vec{c}_T = \vec{a}_R + \vec{b}_R$. If the complexes retained their average $\bar{3}$ symmetry, they would be body centered. Thus the appearance of forbidden reflections of the type $h + k + l \neq 2n$ in the triclinic lattice would be indicative of the postulated model for the antiferrodistortive salt. The intensities at these lattice points were therefore recorded at 20 K in the hemisphere below $2\theta = 20°$, and of the 95 points examined, only 11 had an intensity of $4\sigma(I)$ or greater, one being 10 times its standard deviation. The evidence for the doubled cell from diffraction data is therefore rather weak.

(iii) Antiferrodistortive $Cu(C_5H_5NO)_6(ClO_4)_2$ Crystals from DMF. The scan profiles of three reflections, 666, 120, 350, recorded in this lattice showed no change in shape between 298 and 20 K, in contrast to those observed in (i) and (ii). Compare part C of Figure 2 with parts A and B. The $\bar{3}$ diffraction symmetry and the extinction condition $-h + k + l = 3n$ (hexagonal lattice) were verified by measuring all reflections in the shell $20 \leq 2\theta \leq 40°$. Therefore, within the range 20–298 K, there was no evidence in the diffraction data for departure from the rhombohedral lattice that characterizes the high-temperature phase of the $Cu(C_5H_5NO)_6^{2+}$ salts.

Table I. Summary of Neutron Diffraction Data Collection and Refinement

A. Unit-Cell Data at 20 K	
space group	$R\bar{3}$
λ, Å	1.0422
a, Å	12.260 (1)
c, Å	18.798 (2)
Z	3
d_{exptl}, g/cm^3	1.696
B. Description of Crystal	
faces	$(1\bar{1}0)$, $(\bar{1}10)$, $(\bar{1}10)$ $[(\bar{2}30)$, $(1\bar{1}8)$, $(\bar{2}16)$, $(125)]$[a]
vol, mm^3	5.48
abs coeff,[b] cm^{-1}	1.55
C. Intensity Data Measurement	
temp, K	20.0 (3)
$[(\sin\theta)/\lambda]_{max}$, Å^{-1}	0.79
scan width (2θ), deg	$(\sin\theta)/\lambda \leq 0.48$ Å^{-1}, 3.6; $(\sin\theta)/\lambda > 0.48$ Å^{-1}, $(2.52 + 2.62 \tan\theta)$
av no. of steps/scan	65
counting time/step, s	2
standards	two ($\bar{6}51$ and $1\bar{6}5$) measd every 3 h, no significant variation with time
no. of observns	2037
no. of unique observns	1938
agreement $R = \Sigma\lvert F_o^2 - \bar{F}_o^2\rvert/\Sigma\bar{F}_o^2$	0.0147
D. Refinement	
function minimized	$\Sigma w(F_o^2 - F_c^2)^2$
weights (w)	$[\sigma_c^2(F_o^2) + (0.01F_o^2)^2]^{-1/2}$, where $\sigma_c^2(F_o^2) = (\sin 2\theta)\sigma_c^2(I)$
no. of observns (NO)	1938
no. of parameters (NP)	127, 142[c]
$R(F^2) = \Sigma\Delta/\Sigma F_o^2$[d]	0.049, 0.041[c]
$R_w(F^2) = [\Sigma w\Delta^2/\Sigma(wF_o^2)^2]^{1/2}$	0.055, 0.047[c]
$S = [\Sigma w\Delta^2/(NO - NP)]^{1/2}$	1.57, 1.33[c]
final diff map, largest $\lvert\Delta\rho\rvert$[e]	2.4, 0.67
isotropic extinction parameter $\times 10^4$[f]	0.054

[a] The faces listed within the brackets are approximations to fracture planes. [b] Calculated by assuming the mass absorption coefficient of chemically bonded hydrogen (μ/ρ) to be 23.9 cm^2/g.[16] [c] Second values listed refer to the results of the refinement including the fractional DMF molecule. [d] $\Delta = \lvert F_o^2 - F_c^2\rvert$. [e] Given as a percentage of the peak height of N in the ligand molecule. [f] Type I crystal with Lorentzian distribution of mosaicity.[18]

(iv) Structure Analysis of the $Cu(C_5H_5NO)_6(ClO_4)_2$ Crystals from DMF. The unit-cell parameters given in Table I were determined by a least-squares fit of $\sin^2\theta$ values for 32 reflections distributed over the lattice in the range $48 \leq 2\theta \leq 60°$. The intensity data were measured by $\theta/2\theta$ step scans through the Bragg peaks, with scan widths chosen so that of the total number of points sampled, ~10% at each end of the scans, provided reliable estimates of the background values. All nonequivalent reflections of the obverse rhombohedral lattice were recorded below the $(\sin\theta)/\lambda$ limit of 0.79 Å^{-1}. Additional experimental details are given in Table I. For each reflection, the integrated intensity (I) and variance $(\sigma_c^2(I))$ were evaluated from $I = C - B$ and $\sigma_c^2(I) = C + k^2B$, with the count C taken in the central 80% of the scan and the background B estimated from the two outer 10% parts (i.e., $k = 4$). Lorentz and absorption corrections[14,15] were applied, and symmetry-equivalent measurements were averaged to give the 1938 observations used in the refinement. The reflections were subsequently

(14) de Meulenaer, J.; Tompa, H. *Acta Crystallogr.* **1965**, *19*, 1014.
(15) Templeton, L. K.; Templeton, D. H. "Abstracts", A. C. A. Meeting, Storrs, CT, 1973; p 143.
(16) Koetzle, T. F.; McMullan, R. K., unpublished results, 1979.

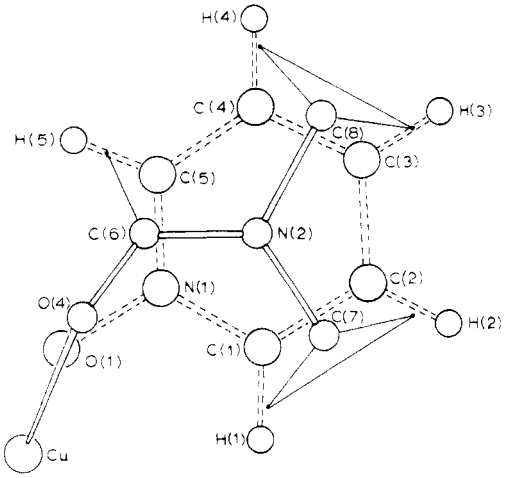

Figure 3. Relative orientations of the C_5H_5NO ligand and DMF molecule in crystals of the perchlorate complex grown from DMF. The regions occupied by the DMF hydrogen atoms are indicated.

reindexed in the hexagonal lattice in order to facilitate computations.

Least-squares refinement was initiated with atomic positions obtained from the reported[4] room-temperature X-ray structure (transformed to the hexagonal cell) and assumed uniform isotropic thermal factors of $U = 0.02$ Å^2. The neutron coherent scattering lengths used were taken from Koester.[17] The refinement conditions are summarized in Table I. The indices of fit at convergence for the 1938 observations were $R(F^2) = 0.049$, $R_w(F^2) = 0.055$, and $S = 1.57$, values which were less satisfactory than expected for the quality of the data. An examination of the ΔF map after convergence revealed that the structure model was incomplete, peaks of low but significant scattering density being found in the region of the pyridine oxide ligand. The configuration of the highest five positive peaks was that expected for the non-hydrogen atoms of a DMF molecule with its oxygen atom coordinated to the copper atom, as depicted in Figure 3. There was no clear evidence of the seven hydrogen atoms in the negative ΔF map, and they were omitted from the final model. The statistical weight of DMF in the structure was estimated by comparing the above peak heights with those observed in the F map at nuclear sites in the ligand. Peak height ratios between atoms of the same type were almost equal at a DMF/pyridine oxide value of ~0.025, which was taken for the occupancy factor of the DMF molecule and not varied in the refinement. When the atomic parameters of the DMF molecule were refined together with those of the main model, the shifts in the former were unrealistic due to high parameter correlation existing between sites in near-proximity and greatly different in statistical weights. When the atoms of DMF were refined alone, their positional parameters converged to acceptable values, but the isotropic thermal factors became negative, indicating that the occupancy factor of 0.025 was somewhat too low. In the final refinement of the main part of the structure, the atomic parameters of the DMF molecule were kept fixed at the positions found in the separate refinement and at isotropic averages of the thermal parameters obtained for heavy atoms of the pyridine oxide ligand. The final residuals $R(F^2)$ and $R_w(F^2)$ were 0.041 and 0.047, respectively, and the fit index, S, was 1.33. The R-factor ratio test[19] showed at the 99.5% confidence level that the additional 15 parameters introduced for the DMF molecule provided an improvement in the structure model. Extinction was found to be significant but not severe, with the minimum effective transmission due to extinction being 0.91 for reflection $\bar{1}23$.

The analysis was performed with the crystallographic least-squares refinement (modified to include a secondary extinction parameter) and function and error programs of Busing, Martin, and Levy, the Fourier summation program of Zalkin, and the thermal ellipsoid plot program of Johnson.[20]

(17) Koester, L. In "Neutron Physics"; Hohler, G., Ed.; Springer-Verlag: New York, 1977; p 37.
(18) Becker, P.; Coppens, P. *Acta Crystallogr., Sect. A* **1974**, *A30*, 129.
(19) Hamilton, W. C. *Acta Crystallogr.* **1965**, *18*, 502.
(20) The following programs were used: Busing, Martin, and Levy's ORFLS, a full-matrix least-squares program (1972); Busing and Levy's ORFFE, a function and error program; Zalkin's FORDAP, a Fourier program (1968); Johnson's ORTEP II, a thermal ellipsoid plotting program (1976).

Table II. Final Structure Parameters for $Cu(C_5H_5NO)_6(ClO_4)_2 \cdot 0.150DMF$ at 20 K (Referred to the Hexagonal Cell)

(A) Positional Parameters

atom	x	y	z
Cu	0	0	0
O(1)	0.11031 (8)	0.04472 (8)	0.06364 (5)
N(1)	−0.05333 (5)	0.15179 (5)	0.09977 (3)
C(1)	−0.01014 (7)	0.26244 (7)	0.06524 (4)
C(2)	0.04972 (7)	0.37483 (7)	0.10249 (4)
C(3)	0.06455 (7)	0.37391 (7)	0.17590 (4)
C(4)	0.01711 (7)	0.25832 (8)	0.21013 (4)
C(5)	−0.04183 (7)	0.14802 (7)	0.17104 (4)
H(1)	−0.0244 (2)	0.2538 (2)	0.0086 (1)
H(2)	0.0851 (2)	0.4623 (2)	0.0733 (1)
H(3)	0.1134 (2)	0.4614 (2)	0.2054 (1)
H(4)	0.0258 (2)	0.2509 (2)	0.2668 (1)
H(5)	−0.0828 (2)	0.0548 (2)	0.1940 (1)
Cl	0	0	0.35020 (4)
O(2)	0	0	0.42647 (8)
O(3)	0.00679 (8)	−0.10759 (8)	0.32441 (5)
O(4)[a]	0.1923 (29)	0.1345 (29)	0.0880 (17)
N(2)	0.2588 (10)	0.0010 (10)	0.1353 (6)
C(6)	0.2056 (22)	0.0725 (20)	0.1372 (12)
C(7)	0.3024 (13)	−0.0259 (13)	0.0704 (8)
C(8)	0.2907 (17)	−0.0349 (18)	0.2072 (28)

(B) Thermal Parameters × 10^4 [b]

atom	U_{11}	U_{22}	U_{33}	U_{12}	U_{13}	U_{23}
Cu	53 (3)	53	41 (5)	26.5	0	0
O(1)	131 (3)	86 (3)	238 (4)	24 (3)	−79 (3)	21 (3)
N(1)	105 (2)	79 (2)	142 (2)	27 (2)	−43 (2)	16 (2)
C(1)	154 (3)	82 (3)	113 (3)	48 (2)	−11 (2)	11 (2)
C(2)	134 (3)	82 (3)	127 (3)	48 (2)	19 (2)	5 (2)
C(3)	144 (3)	145 (3)	139 (3)	92 (3)	−33 (2)	−31 (2)
C(4)	162 (3)	177 (3)	113 (3)	107 (3)	−21 (2)	11 (3)
C(5)	116 (3)	129 (3)	155 (3)	54 (2)	−18 (2)	56 (2)
H(1)	501 (11)	230 (7)	178 (7)	164 (8)	−20 (7)	20 (6)
H(2)	395 (10)	161 (7)	280 (9)	106 (7)	56 (7)	62 (6)
H(3)	401 (10)	254 (8)	298 (9)	170 (7)	−110 (7)	−116 (7)
H(4)	485 (11)	427 (10)	195 (8)	277 (9)	−47 (7)	2 (7)
H(5)	354 (9)	241 (8)	331 (9)	111 (7)	−15 (7)	121 (7)
Cl	80 (2)	80	52 (3)	40	0	0
O(2)	170 (4)	170	70 (5)	85	0	0
O(3)	163 (4)	121 (3)	157 (4)	85 (3)	−9 (3)	−48 (3)

[a] The esd's quoted for the positions of atoms O(4), . . ., C(8) were obtained from a refinement cycle in which all other parameters of the model were held fixed. [b] The thermal factors are of the following forms: anisotropic, $\exp[-2\pi^2(a^{*2}h^2U_{11} + b^{*2}k^2U_{22} + c^{*2}l^2U_{33} + 2a^*b^*hkU_{12} + 2a^*c^*hlU_{13} + 2b^*c^*klU_{23})]$; isotropic, $\exp[-8\pi^2U[(\sin\theta)/\lambda]^2]$, assigned to atoms of the dimethylformamide molecule and fixed at a value of $U = 0.016$ Å^2.

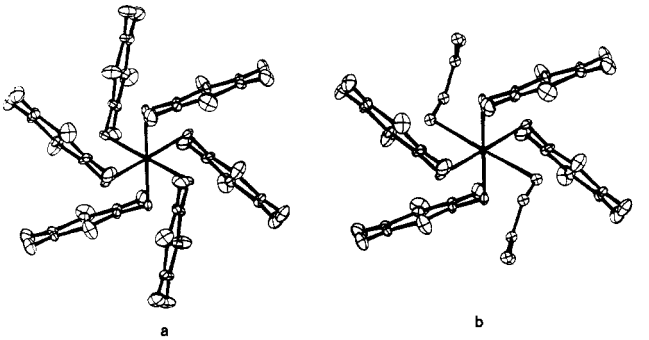

Figure 4. Structures of (a) $Cu(C_5H_5NO)_6^{2+}$ and (b) $Cu(C_5H_5NO)_4(DMF)_2^{2+}$ at 20 K viewed parallel to [111]. Thermal ellipsoids are at the 50% probability level.

The final atomic positional and thermal parameters are listed in Table II, and the molecular parameters are given in Table III. The complexes $Cu(C_5H_5NO)_6^{2+}$ and $Cu(C_5H_5NO)_4(DMF)_2^{2+}$, with di-

Table III. Bond Distances (Å) and Angles (Deg) for $Cu(C_5H_5NO)_6(ClO_4)_2 \cdot 0.150DMF$ at 20 K

	(a) Complex Ion		
Cu-O(1)	2.074 (1)	N(1)-O(1)	1.325 (1)
N(1)-C(1)	1.350 (1)	N(1)-C(5)	1.350 (1)
C(1)-C(2)	1.384 (1)	C(4)-C(5)	1.383 (1)
C(2)-C(3)	1.393 (1)	C(3)-C(4)	1.392 (1)
C(1)-H(1)	1.076 (2)	C(5)-H(5)	1.082 (2)
C(2)-H(2)	1.084 (2)	C(4)-H(4)	1.080 (2)
C(3)-H(3)	1.084 (2)		
$O(1)-Cu-O(1)_3$[a]	90.05 (3)	$O(1)-Cu-O(1)_{\bar{3}}$	89.95 (3)
O(1)-N(1)-C(1)	119.78 (7)	O(1)-N(1)-C(5)	119.14 (6)
C(1)-N(1)-C(5)	121.07 (6)	N(1)-C(1)-C(2)	120.21 (6)
N(1)-C(5)-C(4)	120.40 (6)	C(1)-C(2)-C(3)	119.97 (7)
C(3)-C(4)-C(5)	119.86 (7)	C(2)-C(3)-C(4)	118.48 (7)
H(1)-C(1)-N(1)	114.5 (1)	H(5)-C(5)-N(1)	115.5 (1)
H(1)-C(1)-C(2)	125.3 (1)	H(5)-C(5)-N(1)	124.0 (1)
H(2)-C(2)-C(1)	118.7 (1)	H(4)-C(4)-C(5)	117.8 (1)
H(2)-C(2)-C(3)	121.3 (1)	H(4)-C(4)-C(3)	122.3 (1)
H(3)-C(3)-C(2)	120.6 (1)	H(3)-C(3)-C(4)	120.9 (1)
	(b) Perchlorate Ion		
Cl-O(2)	1.434 (2)	Cl-O(3)	1.446 (1)
O(2)-Cl-O(3)	109.58 (5)	$O(3)-Cl-O(3)_3$	109.36 (5)
	(c) DMF Molecule		
	Cu-O(4) 2.67 (3)		
O(4)-C(6)	1.26 (4)	C(6)-N(2)	1.33 (3)
N(2)-C(7)	1.44 (2)	N(2)-C(8)	1.53 (4)
O(4)-C(6)-N(2)	129.4 (4)	C(6)-N(2)-C(7)	122.5 (3)
C(6)-N(2)-C(8)	116.6 (3)	C(7)-N(2)-C(8)	120.4 (3)

(d) Least-Squares Ligand Plane

$$0.8933X - 0.4129Y - 0.1776Z = 1.747$$

Distances of Atoms from Plane (Å)

N(1)	0.006 (1)	C(1)	−0.008 (1)	C(2)	−0.002 (1)
C(3)	0.006 (1)	C(4)	−0.004 (1)	C(5)	−0.006 (1)
		O(1)	0.005 (1)		

[a] The subscripts 3 and $\bar{3}$ refer to symmetry-related atoms.

substitution assumed, are illustrated in Figure 4 in views down the crystallographic $\bar{3}$ axis.

(c) EPR Measurements. Powder and single-crystal measurements were made at both Q-band (35-GHz) and X-band (9.5-GHz) frequencies on a Varian E-12 spectrometer using Oxford Instruments' continuous-flow cryostats, Models BKESR 12 (for X-band) and BK35ESR (for Q-band), and a locally designed bath cryostat that permitted crystal rotation about two axes. Magnetic fields were measured with a Bruker B-NM12 gauss meter and klystron frequencies with Systron Donner 1037-S and Hewlett-Packard HP 5246L counters. The crystals used for variable-temperature studies were aligned optically and measurements were made at X-band frequency for three mutually orthogonal planes at 10 or 15° intervals. The rotation axes were $[100]_R$, $[01\bar{1}]_R$, and $[100]_R \times [01\bar{1}]_R$. In addition to the measurements that were made on the samples of the mixed-anion complexes and the heavily doped zinc complexes, detailed temperature dependence and line-shape measurements were made at Q-band frequency for a single crystal of the pure perchlorate complex grown from DMF.

(d) Single-Crystal Magnetic Susceptibility Measurements. These measurements were made with a sensitive force magnetometer using a very low frequency (2 Hz) sample position modulation and superconducting pickup coils. Details of the procedure have been described elsewhere.[21] A single crystal of the DMF-grown perchlorate complex obtained from the same batch as those employed in the neutron and EPR measurements was used, and measurements were made from room temperature to 2 K. A Curie–Weiss plot for the region below 100 K is illustrated in Figure 5. The high- and low-temperature regions of the plot have Weiss constants of −30.5 and −2.4 K, respectively, the latter agreeing closely with the value reported earlier.[4]

(21) Snaathorst, D.; Doesburg, H. M.; Perenboom, J. A. A. J.; Keijzers, C. P. *Inorg. Chem.* **1981**, *20*, 2526. Perenboom, J. A. A. J. Ph.D. Thesis, University of Nijmegen, 1979.

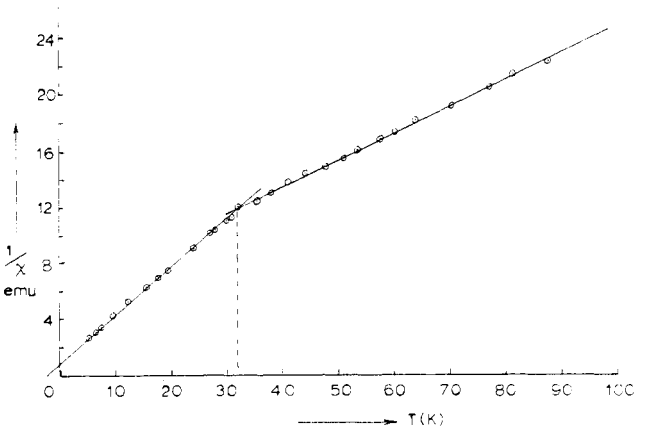

Figure 5. Curie–Weiss magnetic susceptibility plot for a single crystal of $Cu(C_5H_5NO)_6(ClO_4)_2$ grown from DMF.

Results and Discussion

(A) Structural Results. The neutron diffraction measurements on the various rhombohedral phases containing the $Cu(pyO)_6^{2+}$ ion confirm the single-crystal EPR results described in our earlier paper.[9] Thus the ω scans contained in Figure 2 clearly indicate that, for crystals of both the fluoborate salt and the perchlorate salt grown from acetonitrile, three crystallographically distinct domains are produced on passing through the Jahn–Teller transition region, each domain presumably having one of the structures illustrated in Figure 1, parts a and b, for the BF_4^- and ClO_4^- complexes, respectively. In accord with the EPR results, these transitions are reversible and the latter technique shows that, in addition, the domains are related by threefold symmetry. In the case of the BF_4^- salt, there is no apparent change in unit cell size, which is in accord with the ferrodistortive model of Figure 1a, while as indicated in the Experimental Section, a few rather weak reflections expected for the doubled cell in the ClO_4^- salt obtained from acetonitrile were observed, so providing some structural evidence for the antiferrodistortive model depicted in Figure 1b.

Although it would clearly be of interest to obtain the detailed low-temperature structure characterizing the domains of each of these salts, it would be far from a simple matter to assign the individual peaks in the ω scans (even if these were resolvable) to any one of the three reciprocal lattices, unless one domain predominates. While measurement of the total intensity associated with each peak is much more straightforward, an analysis based on such reflections would lead only to an averaged structure, as observed at room temperature, or to a variant of this if the domains differ in size.

In order to assess the magnitude of the additional reflections expected for the antiferrodistortive arrangement, we carried out a calculation of the neutron intensities for a model in which the tetragonal distortions of the complexes are produced by simple translation of the entire pyridine oxide ligands along the Cu–O bond directions. This predicted that a significant number of the low-angle reflections should have a measurable intensity. However, such a simple model for the tetragonally elongated geometry might not be appropriate, for analysis of the low-temperature structure of the ClO_4^- salt grown from DMF suggests that the only ligand atom that is appreciably displaced from its "octahedral" position in forming the tetragonal geometry is the oxygen atom, in which case the majority of the additional reflections might be expected to be rather weak and undetectable.

In contrast to the results described above, however, no such structural change is evident in the ω scans for the crystals of the perchlorate salt grown from DMF and its structure is precisely described by the diffraction data in the space group

Table IV. Thermal Motion Analysis Parameters for $Cu(C_5H_5NO)_6(ClO_4)_2$ at 20 K

(A) Rms Displacements (Å) for the Heavy Atoms along the Thermal Ellipsoid Principal Axes

atom	major	inter	minor
Cu	0.073	0.073	0.065
O(1)	0.182	0.095	0.087
N(1)	0.141	0.089	0.086
C(1)	0.132	0.107	0.090
C(2)	0.125	0.107	0.090
C(3)	0.138	0.105	0.101
C(4)	0.137	0.123	0.092
C(5)	0.147	0.107	0.085
Cl	0.090	0.090	0.072
O(2)	0.130	0.130	0.084
O(3)	0.138	0.126	0.086

(B) Rigid-Body Parameters for the Pyridine *N*-Oxide Ligand[a]

	X	*Y*	*Z*
$T_1 = 0.125$ Å	70.3	58.6	49.0
$T_2 = 0.096$ Å	99.0	38.1	131.6
$T_3 = 0.090$ Å	21.8	70.8	69.2
$L_1 = 3.23°$	64.0	45.8	51.4
$L_2 = 1.86°$	102.4	48.8	141.2
$L_3 = 1.00°$	31.5	73.6	86.8

[a] The ligand coordinate system is oriented such that *X* and *Z* lie in the ligand plane with *Z* along the N–O bond direction.

$R\bar{3}$, if the crystal is assumed to consist either of a single domain or of crystallographically indistinguishable domains that individually possess trigonal symmetry or collectively give this symmetry. While a single-domain model is also consistent with the EPR data, the single-crystal Curie–Weiss plot illustrated in Figure 5 suggests that this form of the ClO_4^- salt undergoes the same type of phase change as the other salts at the Jahn–Teller transition point. We thus conclude that the multiple-domain model best explains all experiments, with the individual domains retaining averaged trigonal symmetry. The thermal motion parameters listed in Table IV and illustrated in Figure 4a support a statistically averaged structure, for these exhibit features similar to those found at room temperature, namely, one having an octahedral geometry for the CuO_6 moiety but having pronounced elongations in the oxygen thermal ellipsoids along the Cu–O bond directions. Since the octahedral geometry required by $\bar{3}$ site symmetry is incompatible with the Jahn–Teller theorem, the room-temperature structure and the shape of the thermal ellipsoids were interpreted in terms of a dynamic average of Jahn–Teller-distorted geometries for the $Cu(C_5H_5NO)_6^{2+}$ ion and the magnitude of the tetragonal distortion was estimated from the thermal parameters. In the present case, however, where the sample temperature (20 K) is lower than the Jahn–Teller transition temperature, the structure presumably represents an equally weighted average of the static tetragonally distorted geometries associated with the three minima in the Mexican-hat potential energy surface characterized by the $E \otimes e$ vibronic coupling. The form of the oxygen ellipsoid in the low-temperature structure is essentially prolate, as opposed to oblate for the room-temperature form, and its major axis makes an angle of 17.5° with the Cu–O bond. A Jahn–Teller radius,[2] R_{JT}, of 0.34 Å is calculated from the magnitudes of the rms vibrational amplitudes along and normal to the Cu–O bond, and this compares with the value of 0.40 Å deduced from the room-temperature data.[9,22] This value of R_{JT} at 20 K, together with the observed averaged Cu–O distance of 2.074 Å, leads to predicted Cu–O distances of 1.980 and 2.274 Å for the tetragonally elongated geometries.

The principal axes of the thermal ellipsoids for the remaining heavy atoms of the ligand do not exhibit the same disparity in magnitude as do those for the oxygen atom and, together with the results of an analysis of the motion of these atoms by the generalized TLS procedure,[23] suggest that the effect of the static disorder is largely incorporated into the oxygen. The fit assuming rigid-body motion gives a mean square ΔU_{ij} of 0.0006 Å^2 compared to the $\sigma(U_{ij})_{obsd}$ of 0.0008 Å^2, with the largest deviation (0.0022 Å^2) occurring for one component of the oxygen atom. While the principal axis of the **T** tensor has almost the same orientation as the major axis of the oxygen atom ellipsoid (the angles for the latter being 58.5, 60.2, and 59.7°, with respect to the ligand *x*, *y*, and *z* axes), its magnitude is much less. This suggests that the distortions to a tetragonal geometry are not produced simply by translations of the ligands parallel to the Cu–O directions (this model was used earlier for the calculation of neutron intensities—vide supra—and for the molecular orbital calculations of EPR parameters[9]) but are accommodated primarily in the libration tensor **L**. No attempt has been made to extract complete positional parameters for the distorted complex from the **T** and **L** tensors.

There is no evidence of excessively high thermal motion or any other form of disorder in the perchlorate ion. Although there is a significant difference between the two Cl–O bond distances, the angles conform well to those expected for an ordered structure.

The other main question that has been considerably clarified by the structure analysis is the confirmation of the presence of appreciable numbers of solvent molecules in the crystals grown from DMF. We had earlier attributed additional lines in the room-temperature EPR spectra of single crystals of the doped complexes grown from DMF/ethanol solution to the presence of solvated complexes, and mass spectroscopic measurements confirmed the presence of trace amounts of DMF in crystals of the pure complexes also. The diffraction results presented here give a much more definitive picture of the mode of coordination of the DMF molecule and of the extent of solvation. On the basis of the analysis of the difference density maps, there is at least 1 molecule of DMF per 40 ligand molecules and this ratio may in fact be larger on the basis of the behavior of the molecule during refinement. With the assumption of monosubstitution, i.e., the formation of $Cu(C_5H_5NO)_5DMF^{2+}$ species, there will be one solvated molecule present for every six or seven parent complexes, while for double substitution, i.e., $Cu(C_5H_5NO)_4(DMF)_2^{2+}$, this ratio will be ca. 1/12. As can be seen from Figures 3 and 4b, the DMF molecule is of the "correct" size and shape such that it can replace a pyridine oxide ligand without any major disruption to the remainder of the complex ion or to the crystal. The resulting long Cu–O bond distance of 2.67 Å means that the solvated complexes will be strongly tetragonally distorted and so would exhibit typical "static" **g**-tensor behavior with $g_\parallel > g_\perp$ at room temperature. This is the situation for the doped complexes, and on the basis of the relative EPR intensities, the substituted species occur to an extent of 1/8 to 1/10 relative to the hexakis complex $Cu(C_5H_5NO)_6^{2+}$, ratios which are quite compatible with the diffraction results.

(B) EPR Results. (i) Pure Complexes. In our previous paper we described single-crystal and powder spectra for the fluoborate complex and noted some apparent discrepancies with regard to the Jahn–Teller transition temperatures both within our own results and in comparison with those of Reinen and Krause.[8] In addition we reported principal **g**-tensor magnitudes for single crystals which differed slightly from those for powders. The single-crystal results quoted were for

(22) Ammeter, J. H.; Burgi, H. B.; Gamp, E.; Meyer-Sandrin, V.; Jensen, W. P. *Inorg. Chem.* **1979**, *18*, 733.

(23) Schomaker, V.; Trueblood, K. N. *Acta Crystallogr., Sect. B*, **1968**, *B24*, 63.

Table V. Summary of Principal g Values and Jahn-Teller Transition Temperatures for $Cu(C_5H_5NO)_6X_2$ Complexes and Their Solvent Dependence

X	solvent	structure[a]	g_1	g_2	g_3	T_{JT},[b] K	T_{measd}, K
BF_4	MeOH[c] (P)[d]	F	2.075	2.079	2.375	90	4.2
	EtOH (P)	F	2.067	2.075	2.369	75–80	77
	MeCN (P)	F	2.071	2.073	2.374	70–75	4.2
	DMF (S)	F	2.089	2.096	2.344	45–50	4.2
ClO_4	MeOH[c] (P)	AF	2.225	2.235	2.083	77	4.2
	MeCN (S)	AF	2.219	2.239	2.081	55–60	4.2
	DMF (S)	AF[e]	2.192		2.168	32[f]	4.2
NO_3	EtOH (S)	AF[g]				45–50	
	EtOH (S)[h]	F	2.072	2.088	2.337		295
	DMF (S)	AF	2.223	2.235	2.081	25–30	4.2
	DMF (S and P)	AF	2.19		2.17		4.2

[a] F = ferrodistortive, AF = antiferrodistortive. [b] T_{JT} = Jahn-Teller transition temperature. These are not sharply defined, the midpoints of the five degree ranges quoted corresponding to approximately equal intensities of high- and low-temperature signals. [c] Results from ref 8. [d] P denotes results from powder samples, and S, results from single-crystal spectra. The g values quoted for the latter are averaged over the three domains. [e] Assumed to be antiferrodistortive on the basis of magnetic specific heat measurements[4] and results from pair spectra. [f] Obtained from a Curie-Weiss plot. [g] No g values measured. [h] Results for the monoclinic phase, which is pseudoferrodistortive. The g values quoted are for the crystal and were determined at X-band frequency. The two independent molecular tensors are almost aligned and can just be distinguished at Q-band frequency.

samples grown from DMF (or DMF/ethanol) which had a transition temperature of 45–55 K and gave **g**-tensor anisotropies slightly smaller than those obtained from powder spectra of samples grown from ethanol, the relative values being $g_\parallel$(EtOH) > $g_\parallel$(DMF) and $g_\perp$(EtOH) < $g_\perp$(DMF). The actual values for the powder samples were very close to those reported by Reinen and Krause for samples grown from methanol, while the transition temperature was in the region 75–80 K. Since we established that the three-domain ferrodistortive pattern is also relevant for fluoborate crystals grown from ethanol and acetonitrile, we did not carry out complete measurements of all planes to obtain the complete tensors for the three sites, and apart from noting that the signals for one domain tended to dominate the spectrum for the DMF-grown samples (Figure 4ii in ref 9), assumed that the solvent used for crystal growing played a relatively minor role in influencing the low-temperature structural pattern.

However, although this role is not as readily apparent in the EPR behavior of the fluoborate complex as that for the perchlorate complex, it is now clear that these initially discrepant results are directly attributable to the occurrence of solvation during the crystal growing process, and in fact the **g**-tensor differences can be quantitatively accounted for if the extent of solvation for the BF_4^- complex is assumed to be the same as that found for the ClO_4^- complex. A summary of the EPR results is presented in Table V, and a comparison of the 4.2 K powder spectra for the pure complexes, given as parts of Figures 6 and 7, illustrates the solvent influence in the case of acetonitrile and DMF, the difference in **g** anisotropy for the fluoroborate salt and the dramatic change in form of the spectrum in the case of the perchlorate salt being clearly evident. The transition temperature, T_{JT}, included in Table V for the DMF-grown perchlorate complex is that determined from magnetic susceptibility measurements. While, as reported earlier,[9] there is no significant change in the **g** tensor from 295 to 4 K, we do not believe that the Jahn–Teller effect is still dynamic down to this temperature and a careful study of the temperature dependence of the line shape and line width was therefore made at Q-band frequency in an attempt to detect the Jahn-Teller transition. However, although there was a variation in the latter by a factor of 2 for the crystal orientation studied (from 53 G at 295 K to 25.7 G at 4.2 K), a minimum was reached at 100 K (12.7 G) and there was no evidence of any sharp change in the region 30–40 K. The line shape was almost pure Lorentzian over the whole temperature range.

From the data in Table V we can draw the following two general conclusions: (a) the Jahn–Teller transition temperatures for the ferrodistortive arrangement (BF_4^- crystal) are higher than those for the antiferrodistortive arrangement (ClO_4^- and NO_3^- crystals), and (b) the solvent used for crystal growing affects the Jahn–Teller transition temperature, the sequence for either ferro- or antiferrodistortive arrangements

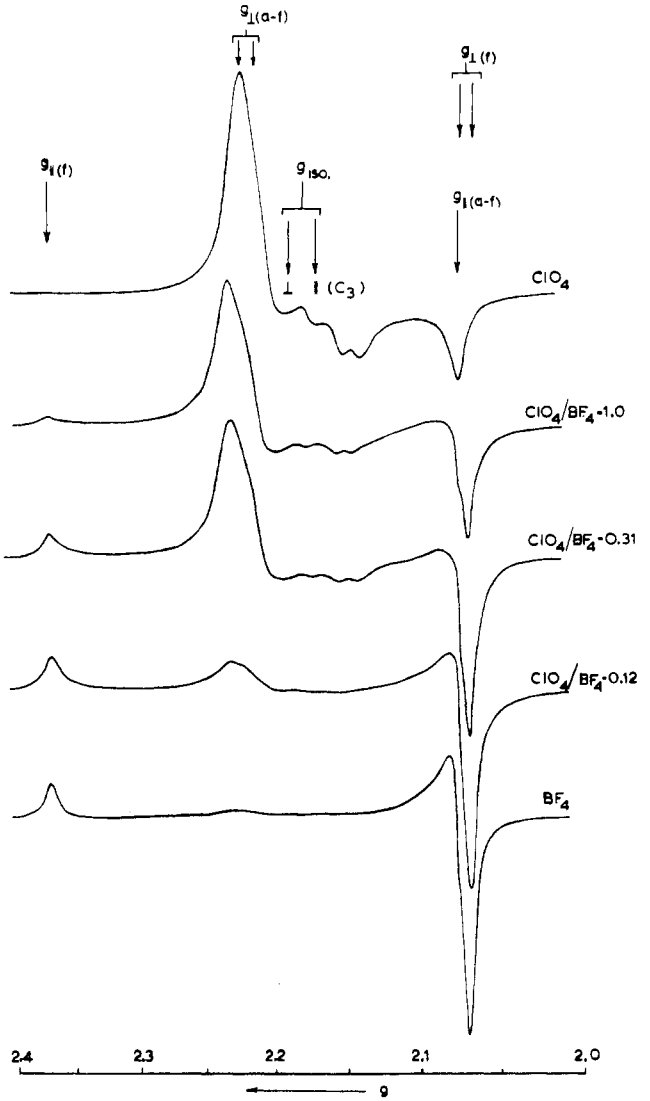

Figure 6. EPR powder spectra, at 4.2 K, of samples of $Cu(C_5H_5NO)_6(BF_4/ClO_4)_2$ containing different anion ratios and grown from acetonitrile.

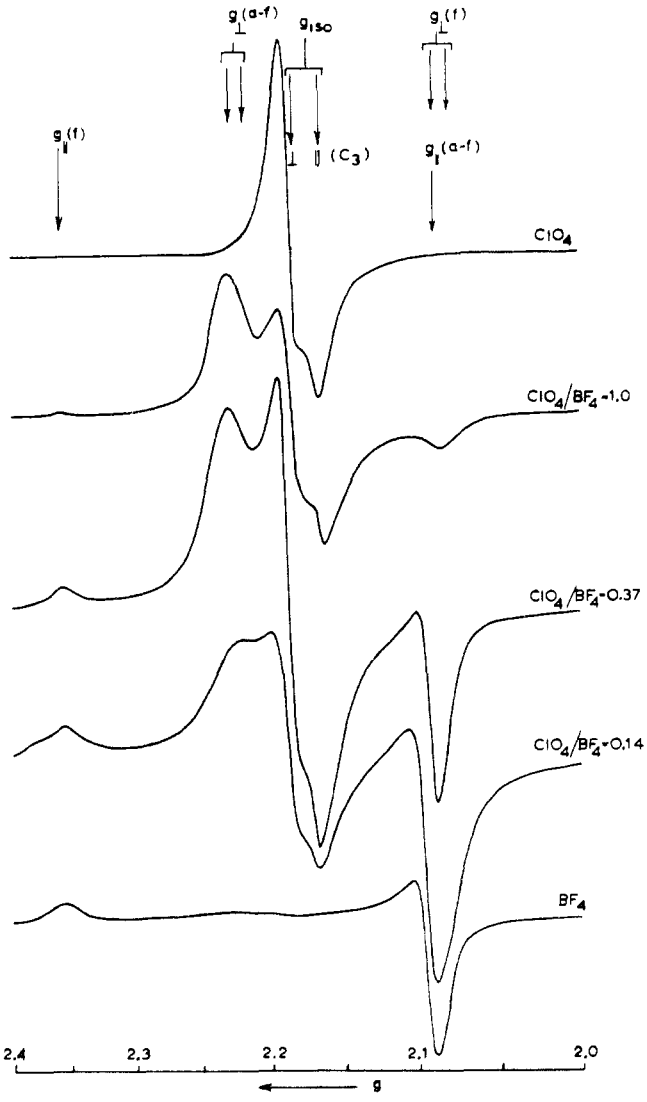

Figure 7. EPR powder spectra, at 4.2 K, of samples of Cu$(C_5H_5NO)_6(BF_4/ClO_4)_2$ containing different anion ratios and grown from DMF.

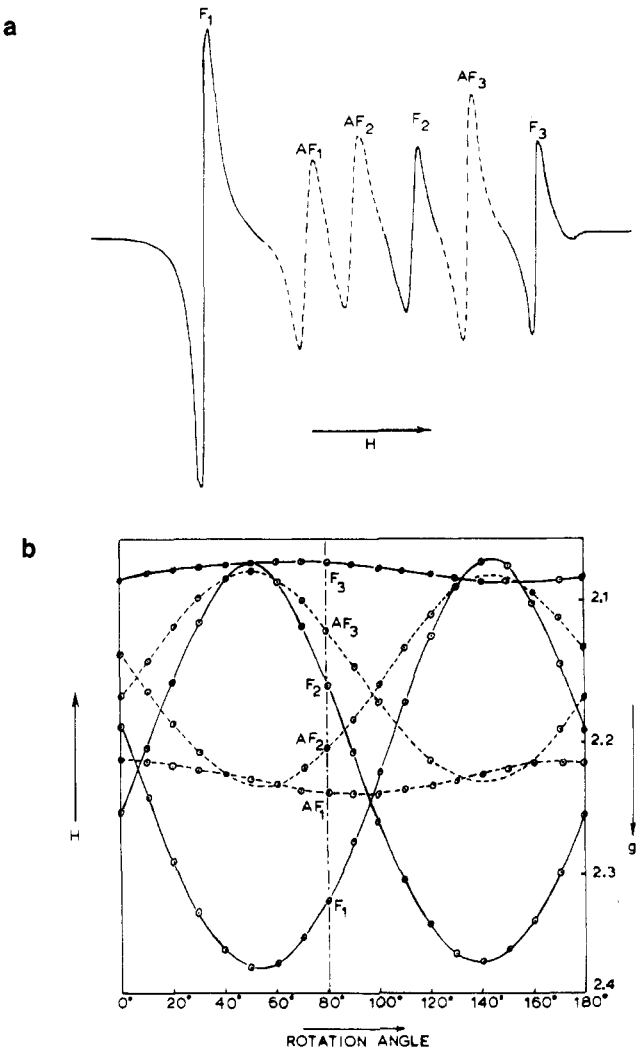

Figure 8. (a) Single-crystal EPR spectrum at 4.2 K of a mixed-anion sample (ClO_4^-/BF_4^- = 0.31) showing both ferrodistortive (F) and antiferrodistortive (AF) sites. (b) Angular variation of sites in the (100) plane for the same crystal. The position of the spectrum in (a) is indicated.

appearing to be methanol, ethanol, acetonitrile, and DMF in order of decreasing temperature, with the most dramatic difference being between DMF and the other solvents. On the basis of the first of these, it appears that the cooperative Jahn–Teller coupling forces are stronger for the fluoborate than for the perchlorate and nitrate salts, while from the second it is evident that the presence of considerable numbers of solvated species decreases the magnitude of the mean interaction energies for both ferrodistortive and antiferrodistortive coupling. The preference for ferrodistortion in the case of the BF_4^- salt is presumably related to the less polarizable nature of this anion compared to ClO_4^- and NO_3^-, and it is suggested by the similar situation existing in the hexanitro complexes,[2] where the type of M^{2+} cation affects the type of ordering. However, as we see from the further EPR results summarized below, this preference is apparently not as strong as the preference of the ClO_4^- salt for antiferrodistortive ordering.

(ii) Mixed-Anion Complexes. In view of the different CJTE's for the fluoborate and perchlorate complexes, we felt it instructive to study samples with mixed BF_4^- and ClO_4^- anions in differing ratios, and some of the resulting powder and single-crystal EPR measurements are summarized in Figures 6–8. Collectively these measurements show that the signals for both ferro- and antiferrodistortive sites are present in all spectra but that, on an intensity basis, the latter tend to predominate. Therefore only those spectra for samples having BF_4^-/ClO_4^- molar ratios ≥ 1 are illustrated.

For the samples grown from acetonitrile, both the principal g values and the transition temperatures for the ferro- and antiferrodistortive signals are very close to those found for the pure fluoborate and perchlorate salts, and a single-crystal analysis confirms this. A complete rotational study of three planes for a sample containing a ClO_4^-/BF_4^- molar ratio of 0.30 shows the spectra contain signals from six sites, three ferrodistortive and three antiferrodistortive, each set having an angular dependence identical with those for the corresponding pure complexes. One of the rotational plots is illustrated in Figure 8, and this is clearly a superposition of the g plots given for plane 1 of each pure crystal in Figure 5 of ref 9. However, the ratio of the total intensities associated with the two sets of sites differs considerably from the molar ratio and, being close to unity, suggests that the cooperative interaction energies leading to the antiferrodistortive arrangement predominate in determining the low-temperature structure.

The mixed-anion samples grown from DMF are more complicated in that not only the signals for the appropriate pure samples, i.e., the near-isotropic (ClO_4^-) and ferrodistortive (BF_4^-) lines, but also the signal corresponding to the $g_{\perp}$ value of the antiferrodistortive arrangement appear in the spectra.

The results for powder samples with varying anion ratios are given in Figure 7, and we note that the g values and transition temperature for the ferrodistortive sites closely parallel the values for the pure fluoborate salt grown from DMF and specifically that the g anisotropy for these sites is smaller than that for the acetonitrile-grown crystals. For anion molar ratios of 1.0 and 0.37, the dominant feature of the powder spectra is the isotropic line. This is also evident in the single-crystal spectra for samples of both ratios, and in the latter, the "normal" antiferrodistortive signals (with $g_\perp > g_\parallel$) account for only a rather small proportion of the total intensity. As for the samples obtained from acetonitrile, the latter is not distributed according to the molar ratio but in this instance is concentrated principally in the isotropic signal and is thus to be associated with a preference for the antiferrodistortive arrangement.

(iii) Doped Systems. As the results of the measurements on the mixed-anion complexes suggest that the antiferrodistortive arrangement is the energetically preferred one for the low-temperature structures, we have undertaken EPR measurements on semidilute crystals of ^{63}Cu in $Zn(C_5H_5NO)_6(ClO_4)_2$ and $Zn(C_5H_5NO)_6(BF_4)_2$ in order to examine the interaction between nearest-neighbor pairs at the microscopic level and to attempt to verify this conclusion. The spectra of crystals containing from 5 to 10% copper are well resolved at low temperature and show weaker lines arising from pairs of neighboring exchange-coupled copper complexes, in addition to the lines arising from isolated complexes. Figure 9 contains two examples of such pair spectra, with the field direction parallel to the principal direction of one of the three sites. In this direction, the high-field part ($g_\perp$) of the pair spectra is buried underneath the complicated spectrum of the isolated complexes and cannot, therefore, be analyzed. A complete evaluation of the low-field part of the pair spectra has not yet been completed, but the following significant qualitative results emerge from these measurements.

1. Fluoborate Complex Grown from Acetonitrile (See Figure 9a). In the $g_\parallel$ region, the spectrum shows the presence of ferrodistortively coupled pairs with the same g value as that of the isolated complex. The two types of pairs that are to be expected are both observed: side-on (large exchange, perpendicular component of effective dipolar interaction along $g_\perp$), which gives rise to the well-known two sets of seven hyperfine lines, separated by the zero-field splitting (A and B in the figure), and head to tail (small exchange, parallel component of dipolar interaction along $g_\parallel$), which gives rise to a complicated pattern of triplet and singlet–triplet transitions. In the region between $g_\parallel$ and $g_\perp$ lines are observed that can be attributed to antiferrodistortively ordered pairs. We discuss these in the next paragraph but conclude from their appearance that the energetic preference for ferrodistortion in the fluoborate salt is only slight, the conditions in the semidilute complex being sufficiently changed from those in the pure salt to permit the occurrence of antiferrodistortive pairs.

2. Perchlorate Complex Grown from Acetonitrile (See Figure 9b). Except for some weak lines in the low-field region which can be attributed to ferrodistortive pairs, all the pair lines in this spectrum originate from antiferrodistortive pairs and occur, therefore, at g values between $g_\parallel$ and $g_\perp$. A full analysis is only possible with the aid of additional Q-band spectra, which will be given in a forthcoming publication.[24] The lines that are clearly resolved in the X-band pair spectrum are assigned to the transitions arising from pairs with a small exchange interaction (elongated axis pointing toward the short axis) and with the parallel component (denoted by A in the figure) or the perpendicular component (A′ in the figure) of the dipolar interaction along the magnetic field direction. We conclude that the preference for antiferrodistortion in the perchlorate salt is large, as is the case in the pure salt.

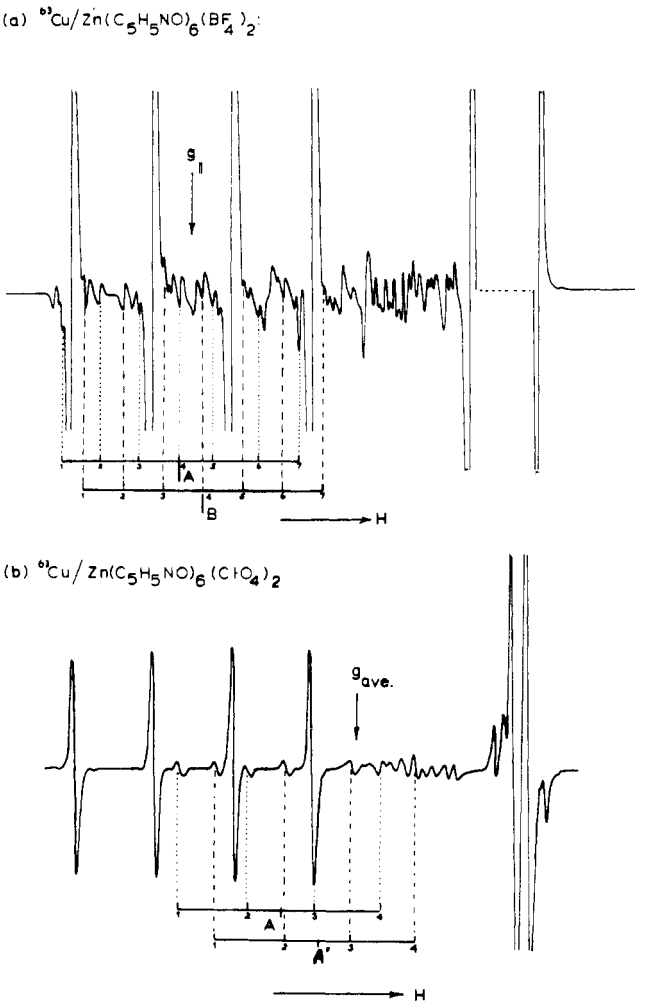

Figure 9. X-Band pair spectra at ~20 K for 10% ^{63}Cu-doped crystals of $Zn(C_5H_5NO)_6X_2$ complexes as indicated. The magnetic field is parallel to g_z ($g_\parallel$) of one of the three equivalent sites.

3. Semidilute Perchlorate Complex Grown from DMF. For this complex, which shows the statically distorted sites at room temperature,[6,7] the spectrum at 4.2 K clearly shows that all pairs are antiferrodistortively oriented as judged from their g values. There is no evidence for ferrodistortive pairs.

(C) Nature of the Low-Temperature Structures. The additional EPR results described in the present paper supplement those reported earlier[8,9] and provide further evidence for the ferro- and antiferrodistortively ordered models of the low-temperature structures of the $Cu(C_5H_5NO)_6X_2$ salts and also of their relative stabilities. On the basis of the neutron diffraction analysis results, it is now clear that solvated species can be incorporated into the structures and that, when this occurs, these can modify the potential energy surfaces leading to different transition temperatures and EPR parameters and do so dramatically when DMF is the solvent.

Now that we have established with reasonable certainty that the same type of antiferrodistortive coupling is involved in the perchlorate salt grown from DMF as in that grown from acetonitrile, it remains for us to devise a model including the solvated complexes that accounts for the retention of apparent trigonal symmetry in this complex, for clearly the earlier model[9] is not applicable.

To do this, we use the experimental observation that, below the phase transition, there is a strong energetic preference for

(24) van Kalkeren, G.; Keijzers, C. P.; Srinivasan, R.; de Boer, E.; Wood, J. S. *Mol. Phys.*, in press.

antiferrodistortion in the perchlorate complex and for ferrodistortion in the fluoborate complex. In both distortions three equally probable types of domains are possible based on the structures depicted in Figure 1. With use of the directions of the tetragonal axes as labels, they are denoted by *x*, *y*, *z* (ferrodistortive) and *xy*, *xz*, *yz* (antiferrodistortive). As can readily be seen, the molecules in the boundary between two different ferrodistortive domains are automatically coupled antiferrodistortively and thus raise the energy of the system. On the other hand, the linkage between two different antiferrodistortive domains can always be such that the molecules in the boundary are also coupled antiferrodistortively with all six nearest neighbors. Therefore, in the perchlorate crystal the formation of small domains does not influence the energy, whereas in the fluoborate crystal the formation of larger domains is energetically favored. The difference in resolution of the neutron reflections below the phase transitions in Figure 2A,B may in part be attributed to this mechanism.

In this model, the effect of the incorporation of relatively large numbers of solvated molecules, each characterized by its fixed tetragonal axis, is easily understood. In the perchlorate crystal, each such molecule can be surrounded by an antiferrodistortive arrangement (domain) that is adapted to the direction of the tetragonal axis of this molecule, and there are two possible arrangements for each axis orientation. While, as noted above, the large number of domains that results does not raise the energy of the system relative to that for a situation with larger domains, for the fluoborate crystal, on the other hand, the formation of small impurity-adapted, ferrodistortive domains would raise the energy appreciably. Therefore, it is to be expected that in the fluoborate crystal the solvated molecules will be incorporated in large domains, leading to a misorientation of two-thirds of them. This yields an exchange-averaged **g** tensor for the domain which differs slightly from that found for the acetonitrile- or ethanol-grown crystals, and it is pleasing to find that the observed changes in the *g* values can indeed be accounted for quantitatively by the presence of one solvated site in every twelve complex molecules.

Since the coupling between different antiferrodistortive domains is also antiferrodistortive, the exchange interaction between the unpaired electrons can proceed over the domain boundary. In the case of small domains, this will lead to an averaging of g_x, g_y, and g_z with equal weight. Such an averaging will produce a near-isotropic signal in the EPR spectrum, which is indeed seen for the DMF-grown crystal of the perchlorate complex, even down to 4 K. It leads also to the retention of apparent trigonal symmetry at low temperatures which is observed in the diffraction experiment. The observation of linear-chain magnetism is accounted for as well with this model, for this does not require the chains to be more than a few members in length or to be oriented in any specific direction.

So far, we have not discussed the nitrate complex. For crystals grown from DMF, both the "normal" antiferrodistortive and the perchlorate type of EPR spectra have been observed (see Table V). At the present time, our only explanation for this, in the framework of the model outlined, is that solvation occurs to differing extents in different crystals (the solubility of the nitrate complex differs appreciably from that of the ClO_4^- or BF_4^- complexes) and that, combined with the Jahn–Teller coupling forces appropriate to the nitrate lattice, this leads to this variable or borderline behavior.

If we turn to the EPR results from the mixed-anion complexes, those for the single crystals show clear evidence for the presence of domains with the same **g** tensors as found for the pure complexes. At first sight, ths is puzzling, as it might be naively thought that, in disordered crystals like these, domains cannot exist and that, in their absence, a random arrangement of distortions with exchange coupling would lead to an isotropic EPR signal. Rejecting the unlikely possibility of segregation of the BF_4^- and ClO_4^- regions in the crystal, we present the following hypothesis to explain the spectra.

In the perchlorate complex, the antiferrodistortive ordering is favored energetically and in the fluoborate complex the ferrodistortive ordering, and as noted earlier, we presume the difference in polarizability of the anions ($ClO_4^- > BF_4^-$) to be the cause of this. In a mixed crystal the anion can, on the average, be thought to have an intermediate polarizability between BF_4^- and ClO_4^-. In such a situation the energetic preference for either ferro- or antiferrodistortion would be reduced. If the reduction is sufficient, then different regions could order in either of the two different ways, their weights being controlled statistically by two factors: (i) the molar ratio of BF_4^- and ClO_4^- ions in the mixed crystal and (ii) the relative values of the reduction in energy, E_F, achieved by ferrodistortion, compared to antiferrodistortion, in a pure fluoborate complex and the reduction, E_{AF}, achieved by antiferrodistortion, compared to ferrodistortion, in a perchlorate complex. The results from the pair spectra and the relative intensities of the sites in the single-crystal mixed-anion spectra strongly suggest that $E_{AF} > E_F$. Further support for this model and for the conclusion that $E_{AF} > E_F$ comes from a study of the mixed crystals grown from DMF. Here, in addition to the ferrodistortive and weak antiferrodistortive spectra, the near-isotropic signal is seen with appreciable intensity, showing that the ordering process is closely similar to that in the pure perchlorate crystal grown from DMF.

Acknowledgment. The neutron diffraction analyses described in this research were carried out at Brookhaven National Laboratory under contract with the Department of Energy and were supported by its Office of Basic Energy Sciences. We wish to thank Mr. Joseph Henriques for his technical assistance with the diffraction measurements. In addition, we thank Mr. Kees Beers of the Physics Department, Nijmegen, The Netherlands, for his help with the magnetic susceptibility measurements. The support of this research by the Scientific Affairs Division of NATO through Grant 1432 is gratefully acknowledged.

Registry No. $Cu(C_5H_5NO)_6(BF_4)_2$, 23013-68-5; $Cu(C_5H_5NO)_6(ClO_4)_2$, 14245-15-9.

Supplementary Material Available: A tabulation of observed and calculated neutron structure factors (11 pages). Ordering information is given on any current masthead page.